Journal of MATERIALS RESEARCH

Article
DOI:10.1557/s43578-024-01364-y

Macro-alignment responses of preosteoblast MC3T3-E1 cells on DCPD-coated β-TCP porous scaffolds: Effect of liquid volume/mass ratio and granular sizes

Ahmed Hafedh Mohammed Mohammed[1,2], Khairul Anuar Shariff[1,6,a], Mohamad Hafizi Abu Bakar[3], Hasmaliza Mohamad[1], Aira Matsugaki[4,5], Takayoshi Nakano[4,5], Intan Nirwana[6]

[1] School of Materials and Mineral Resources Engineering, Universiti Sains Malaysia, Engineering Campus, 14300 Nibong Tebal, Penang, Malaysia
[2] Department of Materials Engineering, College of Engineering, Mustansiriyah University, Baghdad, Iraq
[3] Bioprocess Technology Division, School of Industrial Technology, Universiti Sains Malaysia, 11800 Penang, Gelugor, Malaysia
[4] Division of Materials and Manufacturing Science, Graduate School of Engineering, Osaka University, 2-1, Yamada-Oka, Suita, Osaka 565-0871, Japan
[5] Anisotropic Design and Additive Manufacturing Research Centre, Osaka University, 2-1 Yamada-Oka, Suita, Osaka 565-0871, Japan
[6] Department of Dental Materials, Faculty of Dental Medicine, Universitas Airlangga, Surabaya, Indonesia
[a] Address all correspondence to this author. e-mail: biokhairul@usm.my

Received: 17 February 2024; accepted: 28 May 2024

Extensive assessment of bone-like cell responses towards porous β-tricalcium phosphate scaffolds has shown promising osteoconductivity and biocompatibility. However, the activity of bone-like cells is inhibited due to the formation of dense granule structures and the high formation of dicalcium phosphate dihydrate (DCPD) between dense granules during the setting reaction of macroporous α-TCP or β-TCP granule cement. Hence, this study was carried out to investigate the macro-alignment responses of preosteoblast MC3T3-E1 cells on DCPD-coated β-TCP porous scaffolds by evaluating the effect of acidic volume-to-granular mass ratios (AV/GR) and β-TCP granule sizes (GS) on the scaffolds via a setting reaction. The fabricated porous scaffolds were first characterised using Scanning Electron Microscope (SEM), X-ray Diffraction (XRD), Fourier-Transform Infrared (FTIR), porosity, and compressive strength. Then, in vitro tests using preosteoblast MC3T3-E1 cells were performed to determine the macro-alignment of cell responses towards scaffolds. The results imply that the GS and pore size formation inside the DCPD-coated β-TCP porous scaffolds affected the macro-alignment of preosteoblast MC3T3-E1 surrounding the surface of the fabricated porous scaffold specimens. It was expected that the findings in this study will be a game changer that expedites cell responses in coating-on-ceramic technology.

Introduction

The osteoconductivity and biocompatibility of bone-like cells towards porous β-tricalcium phosphate [β-TCP: $Ca_3(PO_4)_2$] scaffolds have been extensively investigated and have shown desirable outcomes [1–4]. However, the bone-like cell responses in large bone defect areas should be expedited to facilitate rapid bone regeneration. The macro- and micropore formations of calcium phosphate (CaP) scaffold significantly stimulate cell responses during bone remodelling [5–10]. Meanwhile, the CaP scaffolds are attractive materials for the bone remodelling process [11]. Since β-TCP is one of the CaP materials that can be resorbed and replaced to form a new bone by osteoclasts-osteoblasts interactions [12, 13]. Therefore, various techniques have been proposed to fabricate β-TCP porous scaffolds with balanced porosity, pore size (PS), and mechanical strength. These methods also improve the osteoconductivity of β-TCP porous scaffolds driven by the bone-like cell responses [14–18]. Likewise, other studies discovered that the appropriate amounts of dicalcium phosphate dihydrate (DCPD) coated on porous and dense β-TCP granules successfully improved bone osteoconductivity and helped fabrication scaffoldings [19, 20]. The DCPD is known as the highest solubility among the CaP materials.

Previously, Shariff et al. used experimental rats and discovered that the osteoconductivity of β-TCP granules had been improved by forming DCPD layers on the surface of dense granules [21]. Furthermore, a recent study conducted by Mohamad Zaidi et al. observed that the DCPD-coated porous β-TCP granules showed higher MC3T3-E1 cell responses than the dense granules [19]. Recent studies reported that the porous structure of scaffolds plays a major role in improving cell adhesion and proliferation [7, 22]. Fukuda et al. successfully formed macropore granule cement by precipitating the DCPD between the β-TCP granule cement via the setting reaction by exposing dense β-TCP granules to the acidic calcium phosphate (ACaP) solution [23, 24]. Likewise, Kien et al. and Shariff et al. investigated the setting ability of α-TCP spheres and foam granules to develop interconnected macropore α-TCP porous granule cement. They discovered that the DCPD bridging crystals, which form interconnected porous α-TCP foam granule cement, induced the formation of DCPD interlocking crystals that facilitated the setting reaction of the porosity. Nevertheless, the α-TCP foam granule cement produced low porosity with a dense granule structure and high formation of DCPD between granules during the reaction that inhibited the activity of bone-like cells [25, 26].

Realising the need to address these drawbacks, this study investigated the macro-alignment responses of preosteoblast MC3T3-E1 cells by assessing the effect of AV/GR and GS on the fabrication of DCPD-coated β-TCP porous scaffolds. The results obtained in this study would offer new insights into understanding the influence of AV/GR and GS on the scaffold characteristics and the bone-like cell responses towards pore and granular sizes.

Experimental

Preparation of porous β-TCP granules

Calcium phosphate slurry powder was prepared by mixing DCPD [$CaHPO_4{\cdot}2H_2O$, Wako, Osaka, Japan] and calcium carbonate [calcite: $CaCO_3$, Wako] powders to achieve a Ca/P molar ratio of 1.5, which is equivalent to the Ca/P molar ratio of β-TCP. The powder mixture was mixed with ethanol in a planetary milling machine (Pulverisette 5; Fritsch GmbH, Idar-Oberstein, Germany) at 200 rpm for 6 h. Following post-drying at 60 °C for 6 h, the dry cake was ground into a powder with an agate mortar and pestle [21]. Then, the obtained powder was added to sodium chloride (NaCl) powder at a ratio of 60:40 (by wt.%) and mixed in a rotating milling machine for 2 h to ensure a homogenous mixture. Finally, the obtained powder was transferred into a stainless-steel mould and compressed at 50 MPa with an oil press machine (MT-50HD; NPa System, Saitama, Japan). Subsequently, the specimens were heated in an electronic furnace to 1100 °C for 6 h at 10 °C/min and left to cool in the furnace until reaching room temperature. Then, the compacted β-TCP specimen was crushed to produce porous β-TCP granules and sieved to obtain two sets of sample sizes of 300–600 μm and 600–1000 μm. The selected sample sizes were then used for further analysis.

Preparation of the ACaP solution

The present study utilised monocalcium phosphate monohydrate [MCPM: $Ca(H_2PO_4)_2{\cdot}H_2O$] (Sigma-Aldrich, Saint Louis, USA) and phosphoric acid (H_3PO_4) (Merck & Co, New Jersey, USA) to prepare the ACaP solution, as reported by Shariff et al. [27]. Accordingly, 2.5 g of MCPM powder was dissolved in 100 mL of H_3PO_4 solution. The ACaP solution should contain 100 mmol/L of Ca^{2+} and 125 mmol/L of PO_4^{3-} (concentration of MCPM was 100 mmol/L).

Scaffold fabrication

The DCPD-coated β-TCP porous scaffolds were fabricated via a setting reaction by exposing the porous β-TCP granules to the ACaP solution. The porous β-TCP granules were placed in a split stainless-steel mould (diameter = 6 mm, height = 3 mm). Then, the ACaP solution was poured onto the porous β-TCP granules according to the respective ratio, as stated in Table 1. The specimen was allowed to react for 8 h to increase the precipitation of plate-like crystals between the granules. Then, the fabricated scaffolds were immersed in acetone to terminate the setting reaction [25].

Characterisation

Morphological surface

The surface morphology of the fabricated specimens was examined using a scanning electron microscope (SEM, S-3400N; Hitachi High Technologies Co., Tokyo, Japan) at a 15 kV acceleration voltage. Prior to SEM observation, the specimens were coated with gold–palladium for 2 min (magnetron sputtering machine MSP-1S; Vacuum Device Co., Ibaraki, Japan). The scaffold structure and pore geometry observed from the SEM

TABLE 1: Acidic volume-to-granular mass ratios of different granular sizes.

Granules size (μm)	Granular mass ratio (g)	Acidic volume (mL)
300–600	0.2	0.3
300–600	0.2	0.6
600–1000	0.2	0.3
600–1000	0.2	0.6

images were utilised to measure the scaffold pore diameters. Using PoroMetric Software that was installed together with the SEM setup, the PS of the porous DCPD-coated β-TCP scaffolds were measured.

Compositional analysis

Compositional analysis of the DCPD-coated β-TCP porous scaffold structure was performed using an X-ray Diffractometer (XRD: D8 Advance; Bruker AXS GmbH, Karlsruhe, Germany) operated at 40 kV and 40 mA. The diffraction angle was continuously scanned in 2θ from 10° to 40° at a scanning rate of 2°/min. A calibration curve for the quantitative analysis of DCPD was also constructed using a mixture of DCPD (2θ = 11.78°) and β-TCP (2θ = 31.2°) [28, 29]. Subsequently, the amount of DCPD formed on the surface of the porous β-TCP was calculated from the integrated area ratio of the XRD peaks using MDI Jade 5.0 software (Materials Data Inc., Livermore, California, USA) [27]. Meanwhile, the DCPD and β-TCP phases were identified and confirmed with those from the International Centre for Diffraction Data (ICDD).

Porosity analysis

The various scaffolds' total porosity was determined using the liquid displacement method based on the technique by Zeng et al. [30]. Primarily, the dry weight of the DCPD-coated β-TCP porous scaffold was immersed in 99% ethanol for 48 h. Ethanol was selected in this method since it could pass through the porous scaffolds without causing the matrix to swell or contract [31, 32]. The total amount of ethanol that penetrated and absorbed into the porous scaffolds throughout the 48 h was calculated using Eq. 1 [31, 32].

$$P(\%) = (W_2 - W_1)/\left({}^{D}ethanol + {}^{V}scaffold\right) \times 100\% \quad (1)$$

where ^{V}scaffold refers to the volume of the wet scaffold, as determined by immersion, and W_2 and W_1 represent the wet weight and dry weight of the scaffolds, respectively. ^{D}Ethanol indicates the density of the ethanol at room temperature.

Compression strength analysis

The mechanical strength of the fabricated scaffolds was determined using an Instron 3369 with a test speed of 1.0 mm/min and 5 kN cell load following the ASTM-D-695–96 standard. The compressive strength measurement was tested five times for each specimen.

Functional group analysis

The functional groups in the porous scaffold specimens were identified using a Fourier-Transform Infrared (FTIR) spectrometer (Perkin Elmer, Spectrum One, USA). Specimens were first crushed into a fine powder using an agate mortar and mixed with potassium bromide (KBr; Sigma-Aldrich, Saint Louis, USA) at a ratio of 1:10 (sample:KBr) [33]. Then, a hand press machine was used to pelletize the sample to form a thin sample disc to ensure good transparency and a short beam path length. The IR spectra were scanned in the 4000 and 400 cm^{-1} range at a resolution of 4 cm^{-1}.

Response of preosteoblast MC3T3-E1 cells surrounding DCPD-coated β-TCP porous scaffold

Preosteoblast MC3T3-E1 cell culture

The biocompatibility of the fabricated (set) DCPD-coated β-TCP porous scaffolds was tested using preosteoblast MC3T3-E1 cells [34–36]. The MC3T3-E1 cells were initially cultured in a Minimum Essential Medium (MEM, Gibco, USA) supplemented with 10% foetal bovine serum (FBS, HyClone, USA) and 1% antibiotic solution (penicillin and streptomycin [P/S]). The cell adhesion and proliferation were then analysed by seeding MC3T3-E1 cells on the selected DCPD-coated β-TCP porous scaffolds. The cells were seeded in a T25 flask containing complete medium-MEM (10% FBS and 1% P/S) and kept in a 5% CO_2 incubator at 37 °C. The medium was replaced with a fresh one every 2 days.

MC3T3-E1 cell sub-culture and seeding onto DCPD-coated β-TCP porous scaffolds

Once the MC3T3-E1 cell culture reached 80–90% confluence, they were sub-cultured and seeded onto the selected DCPD-coated β-TCP porous scaffolds and control (non-set) porous β-TCP granules. Prior to the seeding, the media was discarded, and the T25 flask containing the cell culture was washed with phosphate-buffered saline (PBS). Then, 3 mL of trypsin/ethylenediaminetetraacetic acid (EDTA) (Sigma-Aldrich, USA) was added to the sample and incubated in a 5% CO_2 incubator at 37 °C for 5 min to detach the cells. Next, the cell solution was transferred to a 15 mL tube and added with 3 mL of complete medium-MEM before being centrifuged at 3000 rpm for 15 min. After discarding the suspension, the 20 µl cells were resuspended with complete medium-MEM (10% PBS) for cell counting and observation using a haemocytometer (also known as a Neubauer chamber, which is a microscope slide). Additionally, the cell culture was seeded onto the four specimens of set and non-set β-TCP porous scaffold in 96-well plates, and each well was filled with 200 µL of the complete medium-MEM.

Cell attachment assay

The preosteoblast MC3T3-E1 cell adhesion on the selected DCPD-coated β-TCP porous scaffolds and non-set porous β-TCP granules was evaluated by seeding the MC3T3-E1 cell culture (0.25×10^6 per well) on the fabricated scaffolds in

a 60-mm well plate. Approximately 3.8 mL of the complete medium-MEM was added to each well plate. The prepared well plates were then incubated in a 5% CO_2 incubator at 37 ℃ for 1, 3, 5, and 7 days. The cell adhesion surrounding the porous scaffold surfaces was observed under an inverted microscope (OPTIKA—XDS-3LT, Ponteranica, Italy).

Cell proliferation via the MTT assay

Preosteoblast MC3T3-E1 cells (5×10^4 cells per well) were co-cultured with the selected DCPD-coated β-TCP porous scaffolds and non-set porous β-TCP granules in 96 well plates containing 200 µL of complete medium-MEM. Furthermore, four sets of seeding were prepared and kept in a 5% CO_2 incubator at 37 °C. Then, the 3-(4,5-Dimethylthiazol-2-yl)-2,5- diphenyl tetrazolium bromide (MTT) assay was performed on the sample after 1, 3, 5, and 7 days of the culture period. The MTT solution was prepared by dissolving MTT powder in PBS at a concentration of 5 mg/mL. Prior to the assay, the medium in each well plate was discarded, replaced with 100 µL of fresh complete medium-MEM mixed with 20 µL of MTT, and incubated in a 5% CO_2 incubator at 37 °C for 4 h in the dark. After incubation, the medium was discarded, replaced with 100 µL of dimethyl sulfoxide (DMSO), and incubated in a 5% CO_2 incubator at 37 °C for 30 min until the insoluble purple formazan dissolved into a solution. Finally, the absorbance in each well was measured at 540 nm using an absorbance microplate reader (Elisa Biobase BK-EL-10A, Shandong, China).

Statistical analysis

The quantitative data was expressed as the average standard deviation. One-way Analysis of Variance (ANOVA) was applied to determine the statistical significance of the cell viability between the non-set porous β-TCP granules and the selected DCPD-coated β-TCP porous scaffolds (*$p < 0.05$, **$p < 0.01$, ***$p < 0.001$, and n.s = Not significant). Besides, ANOVA was conducted to compare the differences in DCPD amounts, porosity, and compressive strength of all the fabricated porous DCPD-coated β-TCP scaffolds.

Results and discussion

Physical appearance and surface morphologies

Figure 1 shows the four porous scaffold specimens fabricated through the setting reaction. The porous scaffold specimens were successfully fabricated by exposing the porous β-TCP granules of two different GS (300–600 µm and 600–1000 µm) to the ACaP solution of two different AV/GR (0.3 mL/0.2 g and 0.6 mL/0.2 g). All the porous scaffold samples exhibit a similar appearance.

Figure 2 displays the SEM images of DCPD-coated β-TCP porous scaffold using 300–600 µm porous β-TCP granules exposed to AV/GR of 0.3 mL/0.2 g and 0.6 mL/0.2 g, while Fig. 3 portrays the SEM images of the DCPD-coated β-TCP porous scaffold using 600–1000 µm granules exposed to AV/GR of 0.3 mL/0.2 g and 0.6 mL/0.2 g. The surface morphological observation revealed that the platelet-like crystals were bridged plates between the porous β-TCP granules. In fact, the number of platelet-like crystals formed between 300 and 600 µm granular-sized porous β-TCP using 0.6 mL/0.2 g ratio was higher than that of the 0.3 mL/0.2 g ratio. Although a similar observation was found for the 600–1000 µm granular-sized porous β-TCP, the size of the bridge platelet-like crystals was smaller than those in the 300–600 µm granular-sized porous β-TCP. These findings were consistent with the report by Zaki et al., where larger β-TCP granules slow down the precipitation of platelet-like crystals on their surfaces [37].

Despite having different experimental parameters, specifically the β-TCP GS and the volume of the ACaP solution used to fabricate the DCPD-coated β-TCP porous scaffold, the SEM morphologies obtained in this study were consistent with the previous studies done by Shariff et al. and Wei et al. [25, 38]. Firstly, the present study used porous β-TCP granules, while Shariff et al. and Wei et al. utilised dense α-TCP and β-TCP granules. Nevertheless, both studies observed similar platelet-like crystals precipitated on the β-TCP granular surfaces. Secondly, Shariff et al. reported that the α-TCP foam granule cement could be fabricated after exposure to the ACaP solution at a ratio of 0.2 mL/0.2 g [25]. Comparatively, the present study recorded that the amount of platelet-like crystals precipitated on the porous β-TCP granular surface increased with a higher acidic volume ratio of up to 0.6 mL. A similar trend was observed after replacing the 300–600 µm β-TCP granules with the 600–1000 µm β-TCP granules.

Furthermore, the setting ability of the porous β-TCP granules was contributed by the bridging of the platelet-like crystals, as shown in Figs. 2(b, c, e, and f) and 3(b, c, e, and f). Based on the visual examination, the amount of platelet-like crystals that bridged between the porous β-TCP granular surfaces increased with a higher acidic volume of up to 0.6 mL. Similar bridging phenomena were observed after replacing the smaller β-TCP granules (300–600 µm) with the larger porous β-TCP granules (600–1000 µm). The results are consistent with the physical observation in Fig. 1, indicating that the porous β-TCP granules can be fabricated regardless of the AV/GR and GS.

Phase analysis

Figure 4 depicts the XRD patterns of the 300–600 µm and 600–1000 µm granular-sized porous β-TCP scaffolds exposed to ACaP solution at two different AV/GR (0.3 mL/0.2 g and 0.6

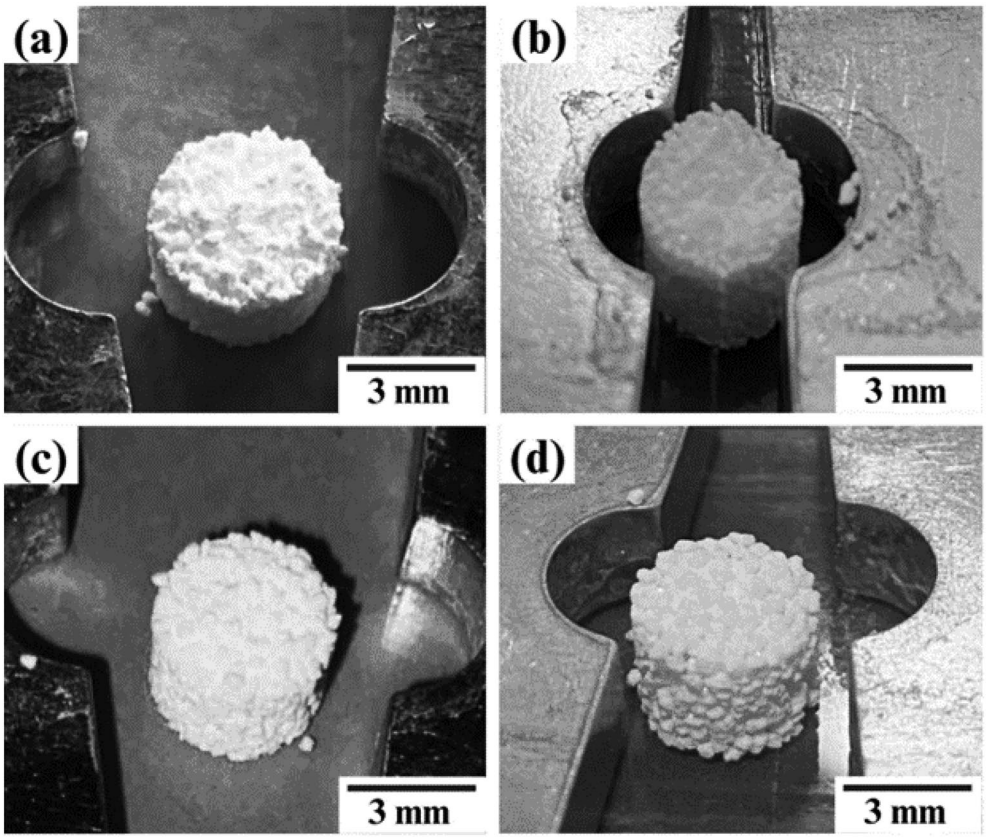

Figure 1: The DCPD-coated β-TCP porous scaffolds were fabricated via the setting reaction using two different GS and two different AV/GR. (a) GS = 300–600 μm, Ratio = 0.3 mL/0.2 g, (b) GS = 300–600 μm, Ratio = 0.6 mL/0.2 g, (c) GS = 600–1000 μm, Ratio = 0.3 mL/0.2 g, and (d) GS = 600–1000 μm, Ratio = 0.6 mL/0.2 g.

mL/0.2 g). The XRD patterns of commercialised β-TCP granules and DCPD were also plotted for comparison. After exposing the porous β-TCP granules to the ACaP solution, a new peak corresponding to DCPD was detected at ($2\theta = 11.7°$), while the peak assigned to β-TCP ($2\theta = 31.2°$) remained, regardless of the AV/GR and GS used in the study. Moreover, the DCPD peaks in the 300–600 μm granular-sized porous β-TCP scaffolds intensified when using a high AV/GR. On the contrary, the peaks belonging to the β-TCP phase remained detected after the phase analysis.

Figure 5(a) shows the amount of DCPD formed inside the 300–600 μm and 600–1000 μm granular-sized porous β-TCP scaffolds exposed to two different AV/GR (0.3 mL/0.2 g and 0.6 mL/0.2 g). The significantly elevated amount of DCPD formation inside the scaffolds was contributed by two main factors: the porous β-TCP granule sizes and the AV/GR used during the setting reaction. As shown in Fig. 5(a), the small porous β-TCP granules produced higher precipitation of DCPD platelet-like crystals between the inter-granular surfaces of the porous β-TCP granules, as evident in Figs. 2(e) and (f). This result was consistent with Zaki et al., who also reported similar findings when using 300–600 μm dense β-TCP granules [37]. The small porous β-TCP granules provide a large surface area that induces the dissolution–precipitation process during the formation of the DCPD coating layer on the surface of the β-TCP granules, as expressed in Eqs. 2 and 3. Besides, the porous β-TCP granules dissolved and supplied sufficient Ca^{2+} and PO_4^{3-} ions in the solution throughout the precipitation-dissolution reaction, as illustrated in Eq. 3 [39]. When the ACaP solution reached its supersaturation level due to the continuous dissolution of Ca^{2+} and PO_4^{3-} ions from the β-TCP granules, Eq. 3 states that DCPD crystals are formed on the surface and inner core of the porous β-TCP granules.

$$\text{Dissolution: } \beta - Ca_3(PO_4)_2 \rightarrow 3Ca^{2+}2PO_4^{3-} \quad (2)$$

$$\text{Precipitation: } Ca^{2+} + H^+ + PO_4^{3-} + 2H_2O \rightarrow CaHPO_4 \cdot 2H_2O \quad (3)$$

Apart from the effect of GS, the AV/GR used during the setting reaction influenced the formation of DCPD. As shown in Table 1, a high volume of ACaP solution would supply a high concentration of Ca^{2+} and PO_4^{3-} ions during the setting reaction. Consequently, the high Ca^{2+} and PO_4^{3-} concentrations surrounded the granules and induced a rapid saturation level of ACaP solution. As a result, the reaction stimulates rapid

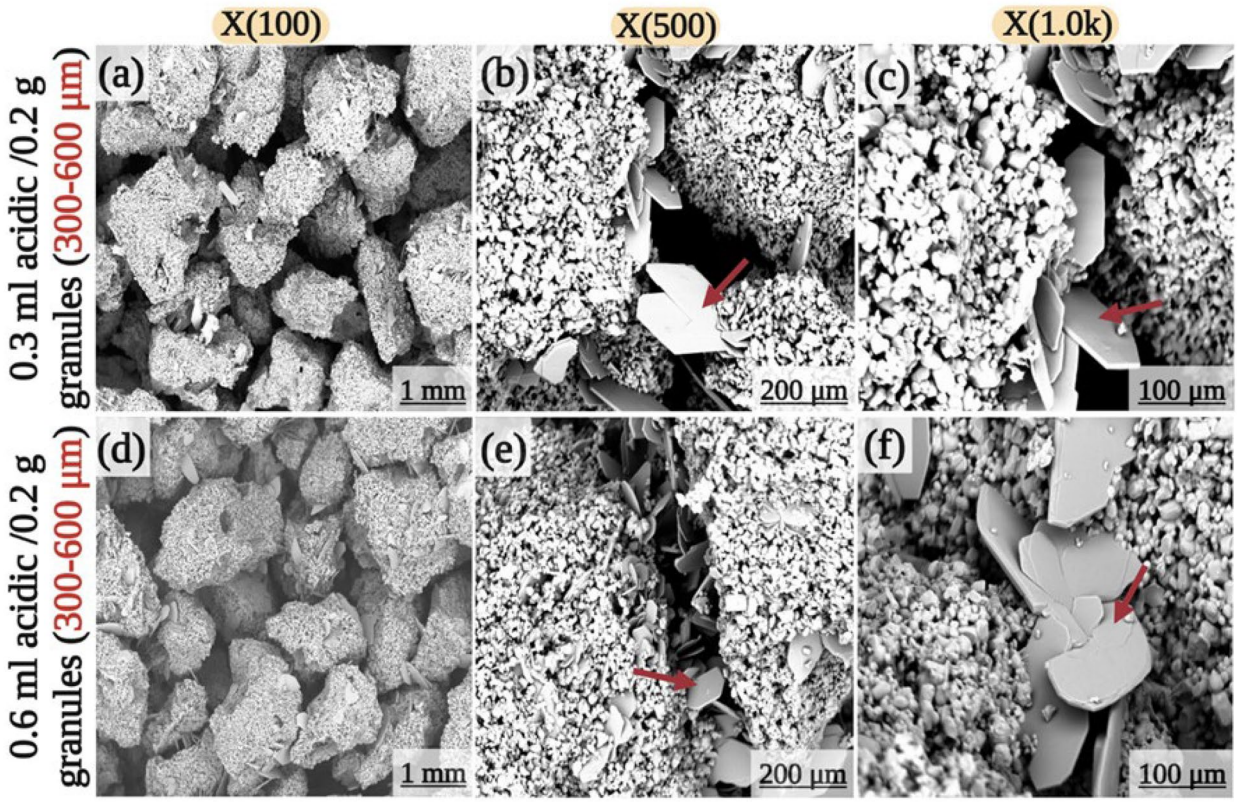

Figure 2: The SEM images of the 300–600 µm granular-sized porous β-TCP scaffold exposed to AV/GR of (a, b, c) 0.3 mL/0.2 g and (d, e, and f) 0.6 mL/0.2 g. (a, d) Low-magnification; (b, c, e, and f) High-magnification.

precipitation of DCPD platelet-like crystals on the surface of the porous β-TCP granules, as described in Eq. 3. These findings are consistent with the SEM morphologies in Figs. 2(d–f) and 3(d–f), which showed a significant formation of DCPD platelet-like crystals after setting porous β-TCP granules of two different GS with AV/GR of 0.6 mL/0.2 g. Based on the confirmed formation of the DCPD platelet-like crystals on the surface of the porous β-TCP granules, the fabricated porous β-TCP scaffolds were denoted as DCPD-coated β-TCP porous scaffolds for further investigation.

Porosity analysis

Table 2 shows the micropore, macropore, and porosity of the 300–600 µm and 600–1000 µm granular-sized DCPD-coated β-TCP porous scaffolds exposed to ACaP solution at two different AV/GR (0.3 mL/0.2 g and 0.6 mL/0.2 g) through the setting reaction. Figure 5(b) depicts the porosity of the four DCPD-coated β-TCP porous scaffold specimens. The results showed that the specimen with a smaller GS (300–600 µm) increased the porosity inside the DCPD-coated β-TCP porous scaffolds. Likewise, the higher ACaP concentration showed lower porosity. Uniquely, the findings contradict the results reported by Zaki et al. and Shariff et al., who recorded that using smaller GS and higher ACaP concentration reduced the porosity values after the setting reaction [25, 37].

These contradictory findings were explained based on two points. The first factor relates to the type of porous β-TCP granules used during the setting reaction process to fabricate the DCPD-coated β-TCP porous scaffolds. Based on the previous findings that used dense granules, the DCPD crystals were formed between the dense granules and the porosity levels were determined based on the size of the formed macropores [25, 37]. For this study, the porosity levels were determined by the number of pores inside the porous granules and macropores formed inside the scaffolds. The second factor involves the macropore and micropore formation inside the DCPD-coated β-TCP porous scaffolds. A significant correlation was observed between the GS and the degree of porosity. As such, smaller β-TCP granules increased the porosity levels due to the higher number of pores inside the scaffolds. Conversely, larger granules exhibit low porosity due to fewer pores inside the scaffolds.

However, a slight decrease in porosity was observed with higher AV/GR, which can be attributed to the increased formation of DCPD crystals during precipitation, consequently altering the pores' dimension. Likewise, the macropore diameter of the scaffolds using larger β-TCP granules (600–1000 µm) was larger than those using 300–600 µm β-TCP granules. The results

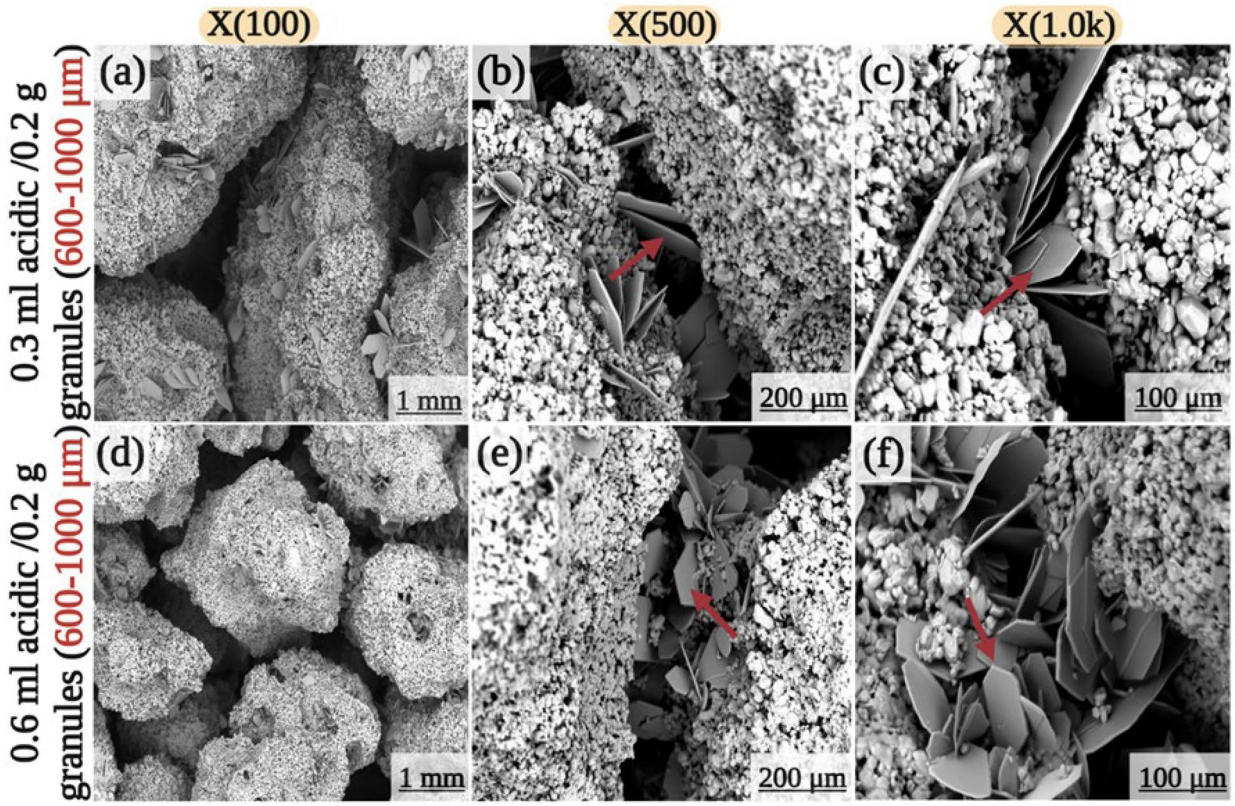

Figure 3: The SEM images of the 600–1000 µm granular-sized porous β-TCP scaffold exposed to AV/GR of (a, b, and c) 0.3 mL/0.2 g and (d, e, and f) 0.6 mL/0.2 g. (a, d) Low-magnification; (b, c, e, and f) High-magnification.

aligned with Shariff et al., who reported the formation of larger macropores using larger granules inside the α-TCP foam granule cement [25].

Mechanical strength analysis

Figure 5(c) shows the compression strength of the 300–600 µm and 600–1000 µm granular-sized DCPD-coated β-TCP porous scaffolds exposed to ACaP solution at two different AV/GR (0.3 mL/0.2 g and 0.6 mL/0.2 g). The graph shows that the compression strength of the specimens increased following the increment of the AV/GR. Moreover, the DCPD-coated β-TCP porous scaffolds fabricated using AV/GR of 0.3 mL/0.2 g recorded a compressive strength of 0.50 MPa (GS of 300–600 µm) and 0.45 MPa (GS of 600–1000 µm). Comparatively, a higher compressive strength of 0.85 MPa (GS of 300–600 µm) and 0.80 MPa (GS of 600–1000 µm) were achieved with DCPD-coated β-TCP porous scaffolds fabricated using AV/GR of 0.6 mL/0.2 g. Despite the enhanced compression strength of the DCPD-coated β-TCP porous scaffolds with higher AV/GR and GS, the compression value difference was statistically insignificant.

The increment of the compression strength values of the DCPD-coated β-TCP porous scaffolds depended on the interlocking phenomenon between the DCPD crystals and the porosity level in the scaffolds. As shown in Figs. 2(b, c, e, and f) and 3 (b, c, e, and f), the developed DCPD platelet-like crystals had interlocked between each other and the porous β-TCP granular surfaces. In fact, increasing the AV/GR to 0.6 mL/0.2 g produced a larger amount of interlocked DCPD crystals between the granular surfaces regardless of the size of the porous β-TCP granules used during the setting reaction.

The findings indicate that the addition of DCPD crystals as an interconnected component between the porous granules significantly influenced the scaffold's structure. The DCPD crystals successfully penetrated the interior of the porous granules and improved the mechanical strength of the DCPD-coated β-TCP porous scaffolds, specifically scaffolds composed of the 300–600 µm β-TCP granules compared to those of 600–1000 µm β-TCP granules. Hence, the total number of pores within the porous granules substantially impacted the precipitation of DCPD, affecting the compression strength of the DCPD-coated β-TCP porous scaffolds.

The mechanical properties of the DCPD-coated β-TCP porous scaffolds were influenced by three distinct conditions. The first condition concerns the GS. The smaller β-TCP granules impacted the precipitation of DCPD crystals between

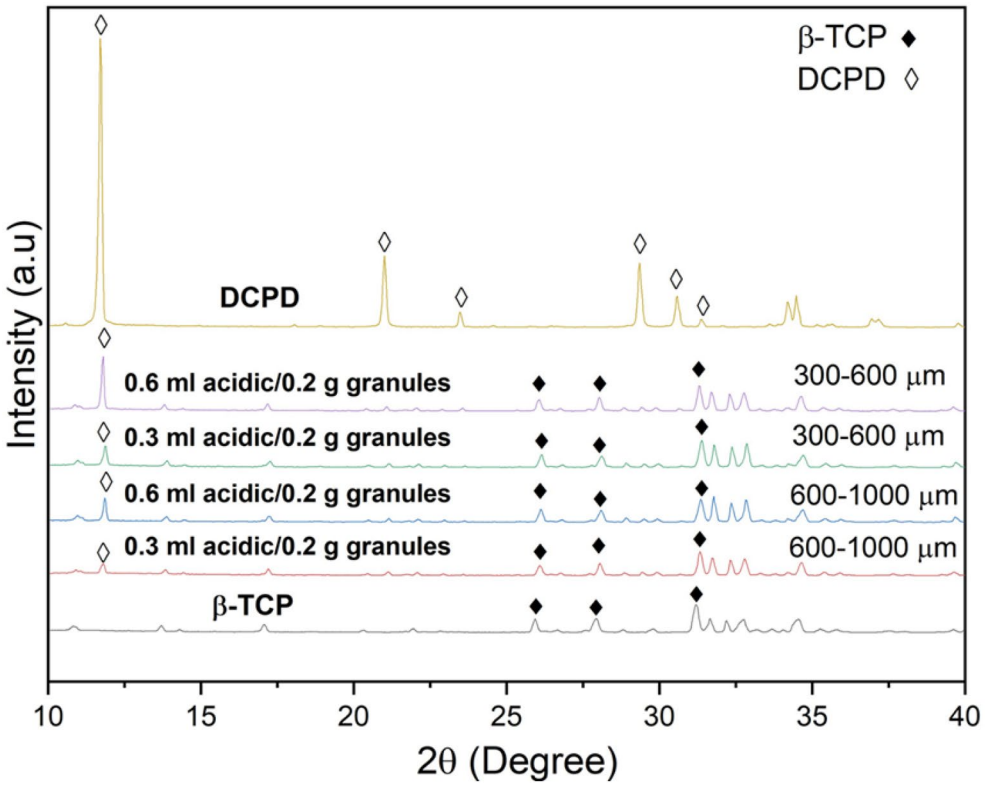

Figure 4: XRD patterns of the 300–600 μm and 600–1000 μm granular-sized DCPD-coated β-TCP porous scaffolds exposed to two different AV/GR (0.3 mL/0.2 g and 0.6 mL/0.2 g) via the setting reaction.

and inside the porous granules. Besides, the use of small granules during the fabrication of porous scaffolds reduced the macropore sizes inside the scaffold, which enhanced the mechanical characteristics of the scaffold compared to those fabricated using larger granules. The trend recorded in this study aligns with the findings reported by Maadani et al., which also revealed an improved mechanical strength of bioceramic scaffolds after incorporating granules with smaller pores [40].

The second condition was related to the total number of granular pores. The usage of small granules essentially affected the pore formation inside the scaffold. Consequently, the increased pore numbers impacted the formation of the DCPD crystal layers within and between the porous granules, which influenced the mechanical strength of the porous scaffolds. Nevertheless, it is generally known that high porosity levels contribute to low mechanical strength. For instance, Flauder et al. discovered that β-TCP scaffolds with 82% porosity recorded a reduced compression strength of 0.4 MPa [41]. A recent study by Ryan et al. also found that the mechanical strength of β-TCP scaffolds increased to 1.4 MPa when the porosity level decreased to 59% [42]. While the mechanical strength of β-TCP scaffolds, which is usually within the range of 0.3–1.4 MPa, may not be suitable for load-bearing applications, the mechanical stability was sufficient for usage in bone regeneration, especially in small bone defects [42, 43].

Finally, the AV/GR ascribes the third condition that affects the mechanical properties of the DCPD-coated β-TCP porous scaffolds. In general, increasing the acidic volume increased the formation of DCPD crystal layers between the granules, as reflected in Figs. 2 and 3. Based on the above conditions, the proposed fabrication method produces DCPD-coated β-TCP porous scaffolds with enhanced mechanical strength and appropriate porosity level, which are essential to support swift and effective bone remodelling.

Chemical functional groups

Figure 6 shows the FTIR results of the 300–600 μm and 600–1000 μm granular-sized DCPD-coated β-TCP porous scaffolds exposed to ACaP solution at two different AV/GR (0.3 mL/0.2 g and 0.6 mL/0.2 g). The results were compared to porous β-TCP granules and commercialised DCPD as a control. According to the FTIR analysis, the PO_4^{3-} functional group was only detected in the porous β-TCP granules at 550–600 cm^{-1} [38]. Interestingly, the PO_4^{3-} functional group remained and continued to be detected regardless of the AV/GR and GS used in fabricating the scaffolds.

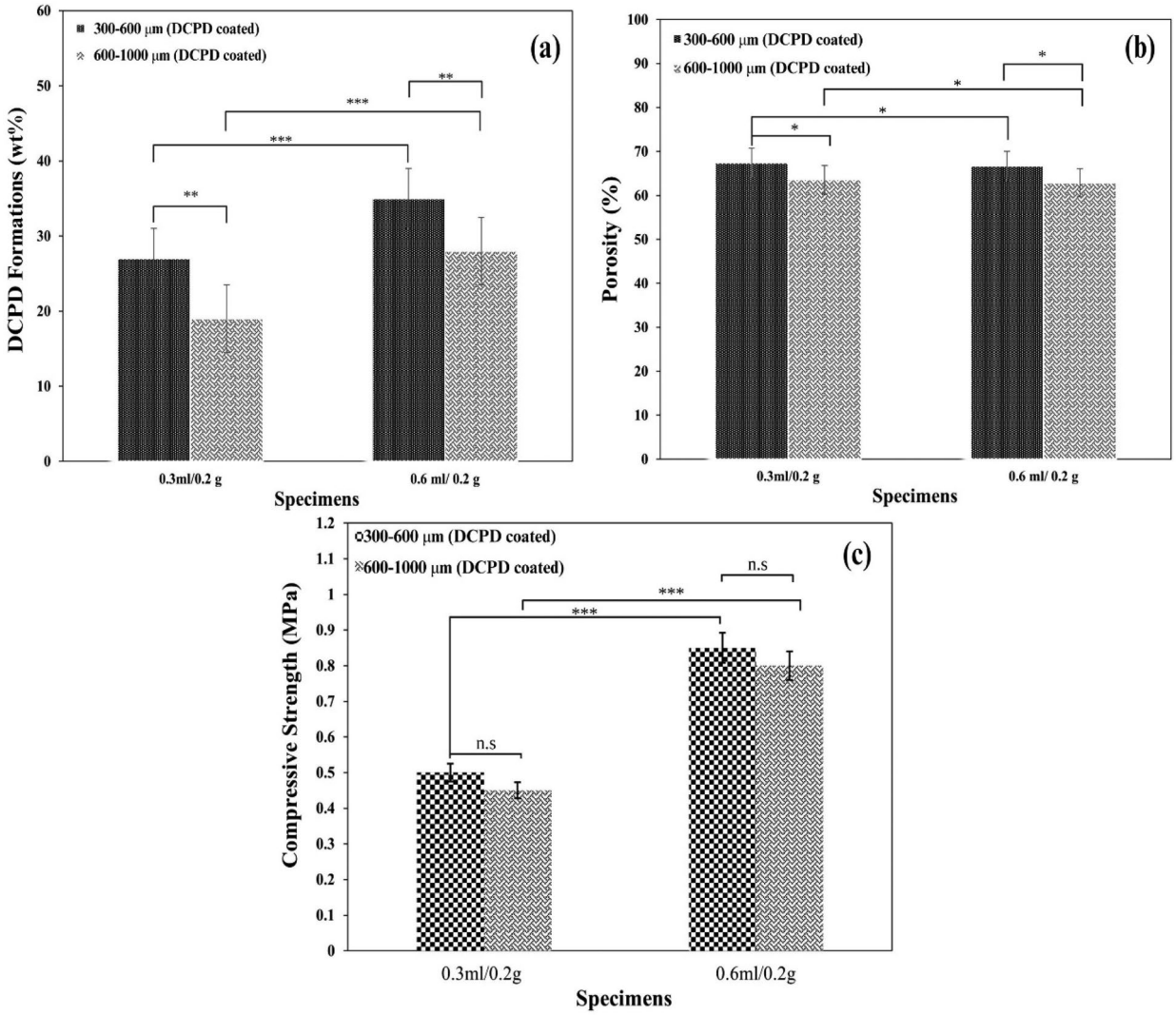

Figure 5: (a) Amount of DCPD formation in the 300–600 μm and 600–1000 μm granular-sized DCPD-coated β-TCP porous scaffolds exposed to two different AV/GR (0.3 mL/0.2 g and 0.6 mL/0.2 g) via the setting reaction. (b) The porosity of the 300–600 μm and 600–1000 μm granular-sized DCPD-coated β-TCP scaffolds exposed to ACaP solution at two different AV/GR (0.3 mL/0.2 g and 0.6 mL/0.2 g) via the setting reaction. (c) The compression strength of the 300–600 μm and 600–1000 μm granular-sized DCPD-coated β-TCP porous scaffolds exposed to ACaP solution at two different AV/GR (0.3 mL/0.2 g and 0.6 mL/0.2 g) via the setting reaction. (Note: n.s = not significant and ***$p < 0.001$, **$p < 0.01$, ***$p < 0.001$).

TABLE 2: Micropore, macropore, and porosity of the 300–600 μm and 600–1000 μm granular-sized DCPD-coated β-TCP porous scaffolds fabricated through the setting reaction using different AV/GR and GS.

Porous DCPD-coated β-TCP scaffolds				
Granule size (μm)	Acidic volume-to-granular mass ratio (mL/0.2 g)	Micropores (μm)	Macropores (μm)	Porosity (%)
300–600	0.3	7.2–7.7	320–350	67.4
300–600	0.6	7.0–7.6	300–340	66.7
600–1000	0.3	7.3–7.9	440–570	63.6
600–1000	0.6	7.1–7.7	410–560	62.9

Conversely, the OH^- functional group was identified at 1638 and 3436 cm^{-1} when porous β-TCP granules were exposed to the ACaP solution. The result also implies the presence of DCPD only in the DCPD-coated β-TCP porous scaffolds. In fact, this finding is aligned with the precipitation process, as shown in Eq. 3. The peak intensity of the OH^- functional group also increased with a higher volume of the ACaP solution during the fabrication of the DCPD-coated β-TCP porous scaffolds.

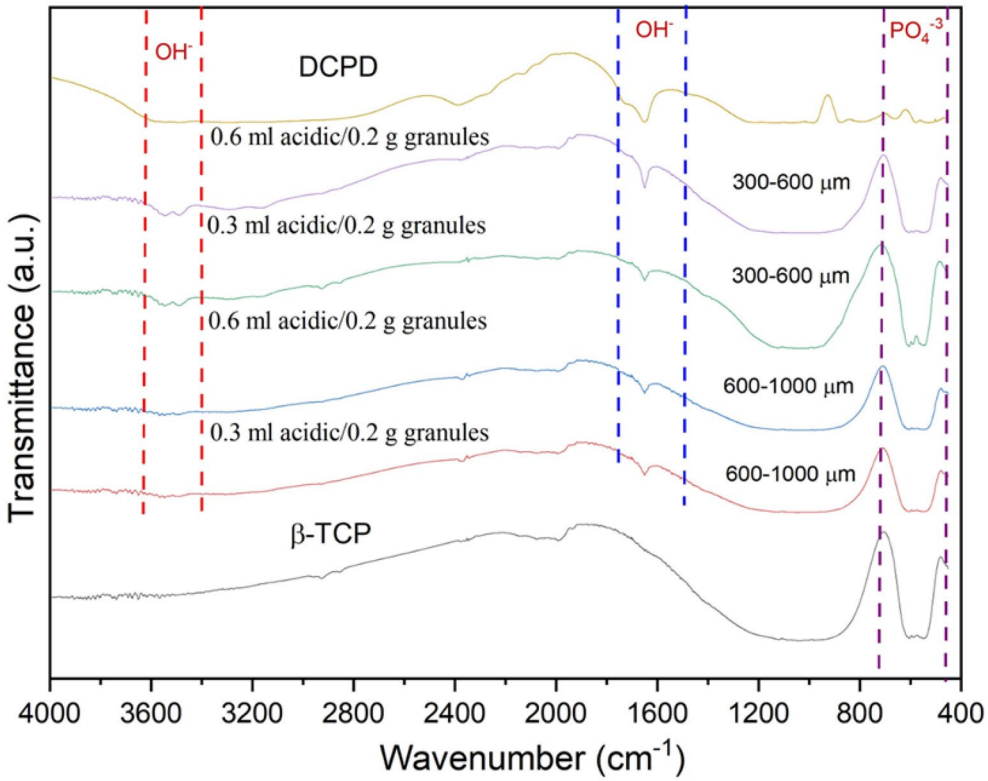

Figure 6: FTIR spectra of the 300–600 µm and 600–1000 µm granular-sized DCPD-coated β-TCP porous scaffolds exposed to ACaP solution at two different AV/GR (0.3 mL/0.2 g and 0.6 mL/0.2 g) through the setting reaction. OH^- and PO_4^{3-} represent chemical functional groups.

Behavioural responses of the preosteoblast MC3T3-E1 cells on the fabricated DCPD-coated β-TCP porous scaffolds

The 300–600 µm and 600–1000 µm granular-sized DCPD-coated β-TCP porous scaffolds exposed to AV/GR of 0.6 mL/0.2 g were selected for the in vitro test using preosteoblast MC3T3-E1 cells due to their outstanding properties, including possessing a higher amount of DCPD crystal layers and robust mechanical strength. Figure 7 illustrates the microscopic imaging of cell attachments surrounding the DCPD-coated β-TCP porous scaffolds compared to those surrounding the non-set porous β-TCP granules (control sample). The cell response towards the specimens was observed after 1, 3, 5, and 7 days of culturing period. The data gathered from the imaging analysis indicate that the cells exhibited adhesion and proliferation on the near surfaces of both the DCPD-coated β-TCP porous scaffold and the control non-set porous β-TCP granules at various time points. It demonstrates that initial cell attachment and subsequent growth can be supported by both types of scaffolds. This is a good discovery because it shows that, in contrast to the uncoated granules, the DCPD coating was not hindering cell attachment. Both scaffold types exhibit consistent cell adhesion and proliferation on their near surfaces, indicating their applicability for tissue engineering applications in which successful tissue regeneration depends on enhancing cell-scaffold interactions.

However, the images showed that the shape of the MC3T3-E1 cells changed when co-cultured on non-set 300–600 µm porous β-TCP granules after 5 and 7 days. The observed phenomenon can be attributed to the increased cell numbers surrounding the non-set porous β-TCP granules. Similarly, the MC3T3-E1 cells became stretched when co-cultured on non-set 600–1000 µm porous β-TCP granules after 5 and 7 days, indicating increased cell numbers surrounding the granules. In comparison, the MC3T3-E1 cells seeded onto the 300–600 µm and 600–1000 µm granular-sized DCPD-coated β-TCP porous scaffolds were located within the macropores of the scaffolds, with the cell shape appearing to be stretched after 3, 5, and 7 days. This observed phenomenon can be attributed to the substantial increase in the quantity of the cells during the specified time intervals.

Besides, the 600–1000 µm granular-sized DCPD-coated β-TCP porous scaffolds exhibited a greater degree of cell elongation compared to that of non-set 300–600 µm β-TCP granules. The MC3T3-E1 cells elongated as the cell density increased, implying that the increased cell numbers influenced the cell stretching due to the narrow space inside the well plate. On the contrary, a low cell density results in a normal

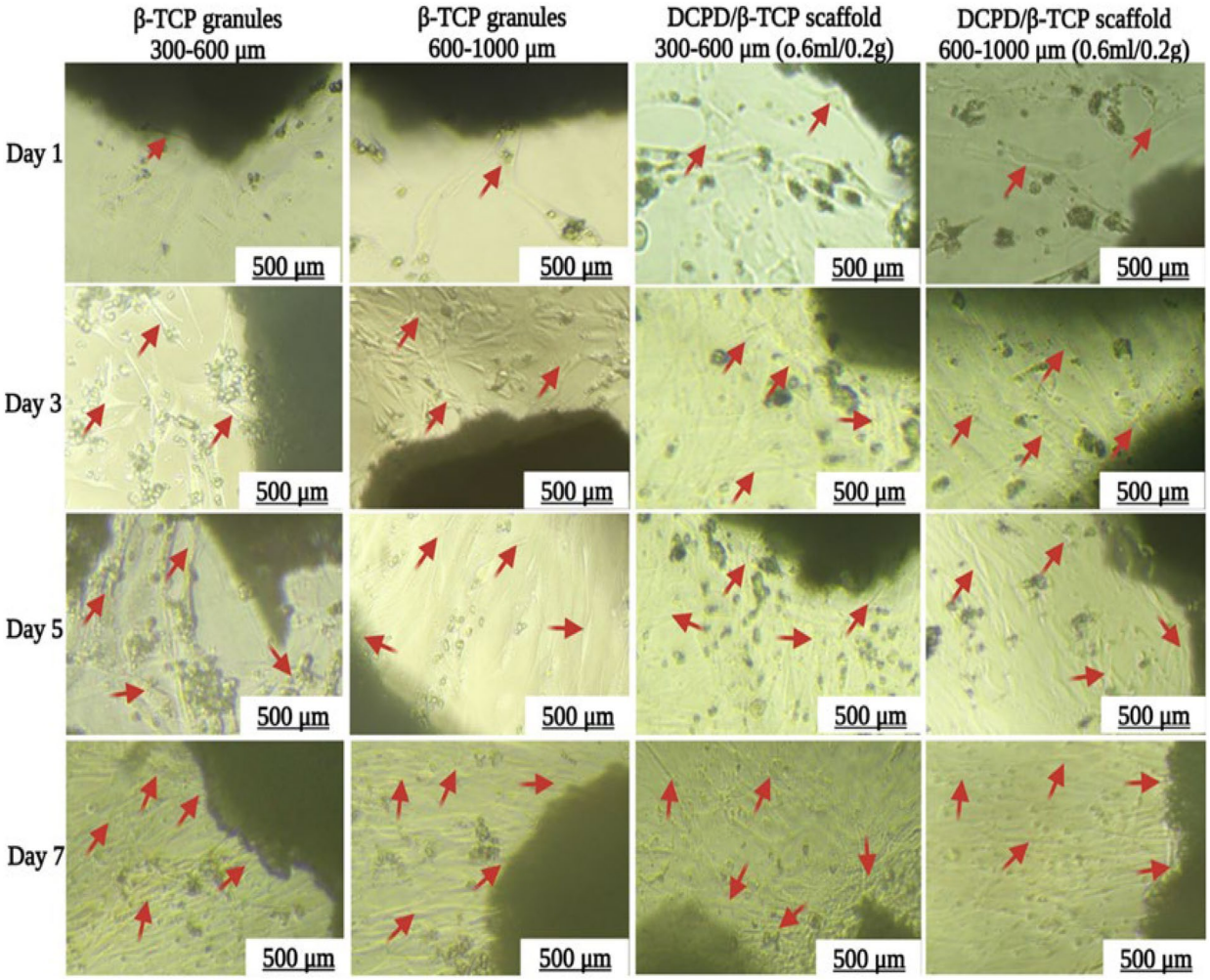

Figure 7: The MC3T3-E1 cell attachment to the 300–600 μm and 600–1000 μm granular-sized DCPD-coated β-TCP porous scaffolds exposed to an acidic volume-to-granular mass ratio of 0.6 mL/0.2 g after 1, 3, 5, and 7 days of culture period. Control porous β-TCP granules were used for comparison. Note: the red arrow refers to the MC3T3- E1 cells and the shadow-like black colour in the figure refers to the surface and debris of the scaffolds.

cell appearance resembling a spider-like shape. The spider-like shape observed at low cell density likely arises from a combination of factors related to cell behaviour and the microenvironment [44]. Therefore, creating an optimal microenvironment for chondrocyte proliferation is crucial due to the insufficient regeneration of cartilage tissue resulting from low cell density [45]. In this study, the direction alignments were shown to be altered at the macropore level during the proliferation of MC3T3-E1 cells, which can be attributed to the increased cell density and proliferation surrounding the porous scaffolds. Furthermore, a recent study reported that at low cell density, the MC3T3-E1 cells showed spider-like shapes and changed to polygonal or spindle shapes due to the growth and proliferation of cells [46]. Likewise, another study found that the MC3T3-E1 cells were elongated spindle-shaped after 3 days of cell culture, which refers to the spreading of cells [47].

Two important factors may affect the change in the cell shape. Firstly, the material composition of the non-set and set porous scaffolds influences cell adhesion and proliferation. Both sets of DCPD-coated β-TCP porous scaffolds showed an increase in cell density compared to non-set porous β-TCP granules. These findings aligned with the study by Shariff et al., who reported that porous β-TCP coated with an appropriate amount of DCPD exhibited enhanced bone osteoconductivity [21]. As a result, the DCPD coatings boosted osteoblast deposition by releasing more Ca^{2+} and PO_4^{3-} ions in the medium [13]. A recent study by Mohamad Zaidi et al. also demonstrated that the porous β-TCP granules coated with DCPD recorded better cell response than DCPD-coated dense β-TCP granules [19].

The second factor refers to the macropores identified within the scaffolds. Specifically, the 600–1000 μm granular-sized DCPD-coated β-TCP porous scaffolds possessed larger macropores (410–560 μm) and more stretched cells than

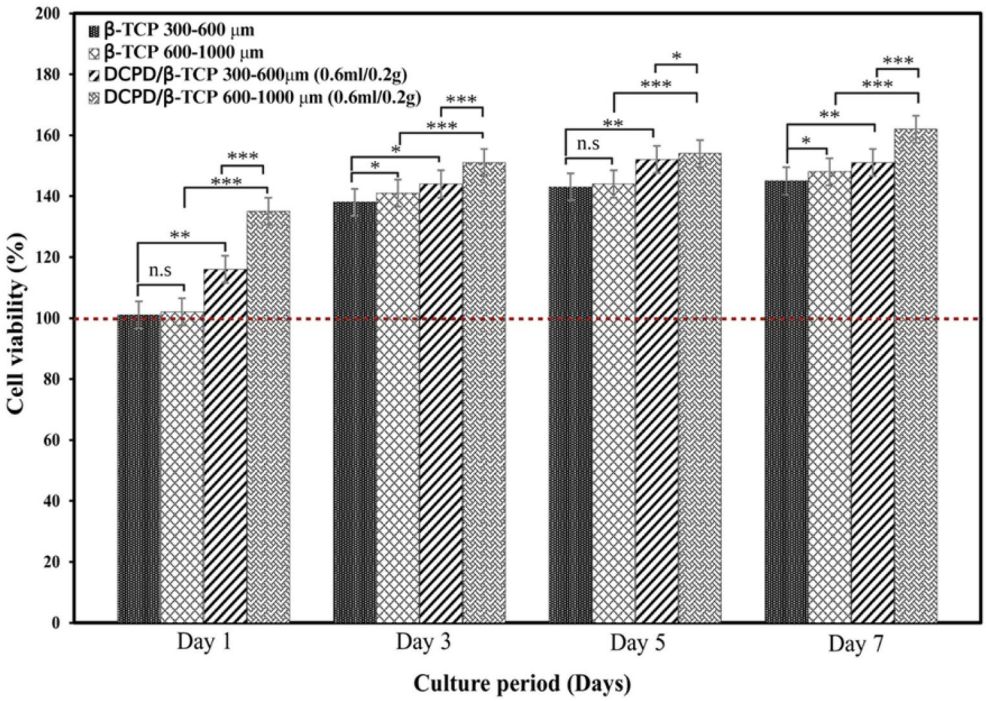

Figure 8: The cell viability of the MC3T3-E1 cells seeded on the 300–600 μm and 600–1000 μm granular-sized DCPD-coated β-TCP porous scaffolds exposed to AV/GR of 0.6 mL/0.2 g. Measured by MTT assay after 1, 3, 5, and 7 days of culture period. (Note: $*p < 0.05$, $**p < 0.01$, $***p < 0.001$ and n.s = not significant). Non-set porous β-TCP granules were used for comparison.

the macropores in the 300–600 μm granular-sized DCPD-coated β-TCP scaffolds (300–340 μm). Likewise, it is vital to note that the MC3T3-E1 cells can proliferate, migrate, and adhere to the scaffold surface due to sufficient macropores and appropriately designed micropore structures [7, 34, 48, 49]. Therefore, the findings in Fig. 7 demonstrate that the 600–1000 μm granular-sized DCPD-coated β-TCP porous scaffolds exhibited a higher cell density, more stretched cell shape, and larger macropores than their 300–600 μm porous scaffold counterparts.

In terms of cell viability and proliferation, the MTT assay allows for the quantitative analysis of cell proliferation based on the live-dead cell determination, demonstrating the cells' ability to attach, and spread successfully [50]. Figure 8 reveals that the absorbance values of the MC3T3-E1 cells seeded onto the fabricated DCPD-coated porous β-TCP scaffolds were higher than that of the controlled porous β-TCP granules. After 1, 3, 5, and 7 days of culturing, the cell absorbance value and cell proliferation of the 600–1000 μm granular-sized DCPD-coated β-TCP scaffolds was higher than other specimens due to their larger micro- and macropore structures and an appropriate amount of DCPD bridged between and inside granules, facilitating the adhesion and proliferation of osteoblast cells [7]. Notably, the amount of DCPD and the number of PS are crucial in cell attachment and proliferation. As such, a larger PS influences the adhesion and proliferation of bone-like cells [7]. Overall, the MTT assay confirmed the absence of any harmful effects associated with using the fabricated porous scaffolds and granules.

Conclusion

The DCPD-coated β-TCP porous scaffolds were successfully fabricated through the setting reaction by exposing porous β-TCP granules to ACaP solution. The high AV/GR (0.6 mL/0.2 g) and larger GS (600–1000 μm) produced porous scaffolds with excellent properties, including large macropore size (410–560 μm), sufficient mechanical strength (0.85 MPa), and appropriate amount of DCPD crystals. Besides, the 600–1000 μm granular-sized DCPD-coated β-TCP porous scaffolds exposed to AV/GR of 0.6 mL/0.2 g supported stronger adhesion and proliferation of preosteoblast MC3T3-E1 cells, which triggered more intense stimulation activity of the cells without any harmful effects associated with the fabricated porous scaffolds.

Author contributions

Each author contributed significantly to the research. Ahmed Hafedh Mohammed Mohammed played a key role in the conceptualization, design, and execution of experiments, particularly in materials characterisation using SEM, XRD, FTIR, porosity and compressive strength analysis. Khairul Anuar

Shariff provided valuable insights into the methodology, oversaw the experimental design, and contributed to the critical review of the manuscript. Other authors, including Mohamad Hafizi Abu Bakar, Hasmaliza Mohamad, Aira Matsugaki, Takayoshi Nakano, and Intan Nirwana, made substantial contributions to the methodology, investigation, critical review of the manuscript and in vitro tests with preosteoblast MC3T3-E1 cells.

Funding

This work was supported by a Universiti Sains Malaysia (USM), Special Short-Term Grant with Project No: 304/PBAHAN/6315702, and Mustansiriyah University for sponsoring the first author to study in Malaysia.

Data availability

Not applicable.

Declarations

Conflict of interest The authors declare that they have no competing interests.

Ethical approval

Not applicable.

References

1. S. Liu, L. Mo, G. Bi, S. Chen, D. Yan, J. Yang, Y.G. Jia, L. Ren, DLP 3D printing porous β-tricalcium phosphate scaffold by the use of acrylate/ceramic composite slurry. Ceram. Int. **47**, 21108–21116 (2021). https://doi.org/10.1016/J.CERAMINT.2021.04.114
2. N. Butler, Y. Zhao, S. Lu, S. Yin, Effects of light exposure intensity and time on printing quality and compressive strength of β-TCP scaffolds fabricated with digital light processing. J. Eur. Ceram. Soc. (2023). https://doi.org/10.1016/J.JEURCERAMSOC.2023.11.046
3. K. Ishikawa, T.S. Putri, A. Tsuchiya, K. Tanaka, K. Tsuru, Fabrication of interconnected porous β-tricalcium phosphate (β-TCP) based on a setting reaction of β-TCP granules with HNO_3 followed by heat treatment. J. Biomed. Mater. Res. A **106**, 797–804 (2018). https://doi.org/10.1002/JBM.A.36285
4. T.S. Putri, K. Hayashi, K. Ishikawa, Bone regeneration using β-tricalcium phosphate (β-TCP) block with interconnected pores made by setting reaction of β-TCP granules. J. Biomed. Mater. Res. A **108**, 625–632 (2020). https://doi.org/10.1002/jbm.a.36842
5. J.E. Won, Y.S. Lee, J.H. Park, J.H. Lee, Y.S. Shin, C.H. Kim, J.C. Knowles, H.W. Kim, Hierarchical microchanneled scaffolds modulate multiple tissue-regenerative processes of immune-responses, angiogenesis, and stem cell homing. Biomaterials **227**, 119548 (2020). https://doi.org/10.1016/J.BIOMATERIALS.2019.119548
6. K. Hayashi, A. Tsuchiya, M. Shimabukuro, K. Ishikawa, Multi-scale porous scaffolds constructed of carbonate apatite honeycomb granules for bone regeneration. Mater. Des. **215**, 110468 (2022). https://doi.org/10.1016/J.MATDES.2022.110468
7. A.H.M. Mohammed, K.A. Shariff, D.A. Wahjuningrum, M.H.A. Bakar, H. Mohamad, A comprehensive review of the effects of porosity and macro- and micropore formations in porous β-TCP scaffolds on cell responses. J. Aust. Ceram. Soc. **2023**, 1–15 (2023). https://doi.org/10.1007/S41779-023-00880-0
8. M. Mohammadi Zerankeshi, S. Mofakhami, E. Salahinejad, 3D porous HA/TCP composite scaffolds for bone tissue engineering. Ceram. Int. **48**, 22647–22663 (2022). https://doi.org/10.1016/J.CERAMINT.2022.05.103
9. V. Mandić, F. Radovanović-Perić, I. Panžić, D. Vrsaljko, Addressing of different synthetic and shaping approaches for β-tri calcium phosphate macro-microporous scaffold fabrication. Ceram. Int. (2022). https://doi.org/10.1016/J.CERAMINT.2022.10.010
10. A. Díaz-Arca, P. Velasquez, P. Mazón, P.N. De Aza, Mechanism of in vitro reaction of a new scaffold ceramic similar to porous bone. J. Eur. Ceram. Soc. **40**, 2200–2206 (2020). https://doi.org/10.1016/J.JEURCERAMSOC.2020.01.045
11. M. Sari, P. Hening, Chotimah, I.D. Ana, Y. Yusuf, Porous structure of bioceramics carbonated hydroxyapatite-based honeycomb scaffold for bone tissue engineering. Mater Today Commun **26**, 102135 (2021). https://doi.org/10.1016/J.MTCOMM.2021.102135
12. K.A. Shariff, M.H. AbuBakar, A. Cahyanto, Behavior of osteoclast cells response on dicalcium phosphate dihydrate layer-coated β-tricalcium phosphate granular. Mater. Sci. Forum **1010**, 549–554 (2020). https://doi.org/10.4028/www.scientific.net/MSF.1010.549
13. A.H.M. Mohammed, K.A. Shariff, M.H.A. Bakar, H. Mohamad, A review on the behavioral responses of osteoclast and osteoblast cells on the near-surface of the bioceramic coating: roles of ions released, solubility, and pH. J. Aust. Ceram. Soc. **58**, 1–13 (2022). https://doi.org/10.1007/S41779-022-00806-2
14. F. Zhang, J. Yang, Y. Zuo, K. Li, Z. Mao, X. Jin, S. Zhang, H. Gao, Y. Cui, Digital light processing of β-tricalcium phosphate bioceramic scaffolds with controllable porous structures for patient specific craniomaxillofacial bone reconstruction. Mater. Des. **216**, 110558 (2022). https://doi.org/10.1016/J.MATDES.2022.110558
15. S. Tarafder, V.K. Balla, N.M. Davies, A. Bandyopadhyay, S. Bose, Microwave-sintered 3D printed tricalcium phosphate scaffolds for bone tissue engineering. J. Tissue Eng. Regen. Med. **7**, 631–641 (2013). https://doi.org/10.1002/TERM.555
16. N.A.S. Zairani, M. Jaafar, N. Ahmad, K. Abdul Razak, Fabrication and characterization of porous β-tricalcium phosphate

scaffolds coated with alginate. Ceram. Int. **42**, 5141–5147 (2016). https://doi.org/10.1016/J.CERAMINT.2015.12.034

17. Y.Z. Shi, J. Liu, L. Yu, L.Z. Zhong, H.B. Jiang, β-TCP scaffold coated with PCL as biodegradable materials for dental applications. Ceram. Int. **44**, 15086–15091 (2018). https://doi.org/10.1016/J.CERAMINT.2018.05.142
18. J. Duan, H. Shao, H. Liu, J. Xu, M. Cong, K. Zhao, T. Lin, 3D gel-printing of hierarchically porous BCP scaffolds for bone tissue engineering. J. Eur. Ceram. Soc. **43**, 2646–2653 (2023). https://doi.org/10.1016/J.JEURCERAMSOC.2023.01.010
19. N.Z. Mohamad Zaidi, A.H.M. Mohammed, M.K. Sujon, K.A. Shariff, M.H.A. Bakar, Behavioural responses of bone-like cells on dense and porous dicalcium phosphate dihydrate-coated β-tricalcium phosphate granules. J. Aust. Ceram. Soc. **2023**, 1–9 (2023). https://doi.org/10.1007/S41779-023-00925-4
20. A.H.M. Mohammed, K.A. Shariff, M. Hafizi, A. Bakar, H. Mohamad, B. My, Fabrication of macro-and micropore forming DCPD/β-TCP porous scaffolds: effect of setting-time reaction and acidic calcium phosphate solution. Iran. J. Mater. Sci. Eng. (2023). https://doi.org/10.22068/ijmse.3402
21. K.A. Shariff, K. Tsuru, K. Ishikawa, Fabrication of dicalcium phosphate dihydrate-coated β-TCP granules and evaluation of their osteoconductivity using experimental rats. Mater. Sci. Eng. C **75**, 1411–1419 (2017). https://doi.org/10.1016/j.msec.2017.03.004
22. A.H.M. Mohammed, K.A. Shariff, M.H. Abu Bakar, H. Mohamad, Recent methods in fabricating porous β-tricalcium phosphate scaffolds: a mini review. Mater Today Proc (2022). https://doi.org/10.1016/J.MATPR.2022.06.498
23. N. Fukuda, K. Tsuru, Y. Mori, K. Ishikawa, Fabrication of self-setting β-tricalcium phosphate granular cement. J. Biomed. Mater. Res. B Appl. Biomater. **106**, 800–807 (2018). https://doi.org/10.1002/JBM.B.33891
24. N. Fukuda, K. Ishikawa, K. Akita, K. Kamada, N. Kurio, Y. Mori, Y. Miyamoto, Effects of acidic calcium phosphate concentration on setting reaction and tissue response to β-tricalcium phosphate granular cement. J. Biomed. Mater. Res. B Appl. Biomater. **108**, 22–29 (2020). https://doi.org/10.1002/JBM.B.34361
25. K.A. Shariff, K. Tsuru, K. Ishikawa, Fabrication of interconnected pore forming α-tricalcium phosphate foam granules cement. J. Biomater. Appl. **30**, 838–845 (2016). https://doi.org/10.1177/0885328215601939
26. P.T. Kien, K. Ishikawa, K. Tsuru, Setting reaction of α-TCP spheres and an acidic calcium phosphate solution for the fabrication of fully interconnected macroporous calcium phosphate. Ceram. Int. **41**, 13525–13531 (2015). https://doi.org/10.1016/J.CERAMINT.2015.07.146
27. K.A. Shariff, K. Tsuru, K. Ishikawa, Regulation of DCPD formation on β-TCP granular surface by exposing different concentration of acidic calcium phosphate solution. Key Eng. Mater. **696**, 27–31 (2016). https://doi.org/10.4028/WWW.SCIENTIFIC.NET/KEM.696.27
28. N. Fukuda, K. Tsuru, Y. Mori, K. Ishikawa, Effect of citric acid on setting reaction and tissue response to β-TCP granular cement. Biomed. Mater. **12**, 015027 (2017). https://doi.org/10.1088/1748-605X/AA5AEA
29. L. Siqueira, F.R. Passador, M.M. Costa, A.O. Lobo, E. Sousa, Influence of the addition of β-TCP on the morphology, thermal properties and cell viability of poly (lactic acid) fibers obtained by electrospinning. Mater. Sci. Eng. C **52**, 135–143 (2015). https://doi.org/10.1016/J.MSEC.2015.03.055
30. S. Zeng, L. Liu, Y. Shi, J. Qiu, W. Fang, M. Rong, Z. Guo, W. Gao, Characterization of silk fibroin/chitosan 3D porous scaffold and in vitro cytology. PLoS ONE **10**, e0128658 (2015). https://doi.org/10.1371/JOURNAL.PONE.0128658
31. A.L. Torres, V.M. Gaspar, I.R. Serra, G.S. Diogo, R. Fradique, A.P. Silva, I.J. Correia, Bioactive polymeric-ceramic hybrid 3D scaffold for application in bone tissue regeneration. Mater. Sci. Eng. C **33**, 4460–4469 (2013). https://doi.org/10.1016/J.MSEC.2013.07.003
32. I.R. Serra, R. Fradique, M.C.S. Vallejo, T.R. Correia, S.P. Miguel, I.J. Correia, Production and characterization of chitosan/gelatin/β-TCP scaffolds for improved bone tissue regeneration. Mater. Sci. Eng. C **55**, 592–604 (2015). https://doi.org/10.1016/J.MSEC.2015.05.072
33. A. Ślósarczyk, C. Paluszkiewicz, M. Gawlicki, Z. Paszkiewicz, The FTIR spectroscopy and QXRD studies of calcium phosphate based materials produced from the powder precursors with different CaP ratios. Ceram. Int. **23**, 297–304 (1997). https://doi.org/10.1016/S0272-8842(96)00016-8
34. X. Ye, Y. Zhang, T. Liu, Z. Chen, W. Chen, Z. Wu, Y. Wang, J. Li, C. Li, T. Jiang, Y. Zhang, H. Wu, X. Xu, Beta-tricalcium phosphate enhanced mechanical and biological properties of 3D-printed polyhydroxyalkanoates scaffold for bone tissue engineering. Int. J. Biol. Macromol. **209**, 1553–1561 (2022). https://doi.org/10.1016/J.IJBIOMAC.2022.04.056
35. J.N. Li, P. Cao, X.N. Zhang, S.X. Zhang, Y.H. He, In vitro degradation and cell attachment of a PLGA coated biodegradable Mg-6Zn based alloy. J. Mater. Sci. **45**, 6038–6045 (2010). https://doi.org/10.1007/s10853-010-4688-9
36. X. Ye, G. Xu, S. Cai, Y. Dou, Y. Zhu, H. Hu, Preparation, surface properties, and MC3T3-E1 cell response of mesoporous hydroxyapatite thin films. J. Mater. Sci. **47**, 3763–3769 (2012). https://doi.org/10.1007/s10853-011-6227-8
37. H.A.M. Zaki, K.A. Shariff, M.H.A. Bakar, M.N. Azmi, Effect of different granular size on the properties of porous β-tricalcium phosphate foam granular cements. Key Eng. Mater. **829**, 23–27 (2020). https://doi.org/10.4028/WWW.SCIENTIFIC.NET/KEM.829.23

38. L.J. Wei, K.A. Shariff, S.A. Momin, M.H.A. Bakar, A. Cahyanto, Self-setting β-tricalcium phosphate granular cement at physiological body condition: effect of citric acid concentration as an inhibitor. J. Aust. Ceram. Soc. **57**, 687–696 (2021). https://doi.org/10.1007/S41779-021-00575-4
39. K. Ishikawa, K. Tsuru, T.K. Pham, M. Maruta, S. Matsuya, Fully-interconnected pore forming calcium phosphate cement. Key Eng. Mater. **493–494**, 832–835 (2012). https://doi.org/10.4028/www.scientific.net/KEM.493-494.832
40. A.M. Maadani, E. Salahinejad, Performance comparison of PLA- and PLGA-coated porous bioceramic scaffolds: mechanical, biodegradability, bioactivity, delivery and biocompatibility assessments. J. Control. Release **351**, 1–7 (2022). https://doi.org/10.1016/J.JCONREL.2022.09.022
41. S. Flauder, U. Gbureck, F.A. Müller, Structure and mechanical properties of β-TCP scaffolds prepared by ice-templating with preset ice front velocities. Acta Biomater. **10**, 5148–5155 (2014). https://doi.org/10.1016/J.ACTBIO.2014.08.020
42. E. Ryan, S. Yin, Compressive strength of β-TCP scaffolds fabricated via lithography-based manufacturing for bone tissue engineering. Ceram. Int. **48**, 15516–15524 (2022). https://doi.org/10.1016/J.CERAMINT.2022.02.085
43. J. Wieding, A. Fritsche, P. Heinl, C. Körner, M. Cornelsen, H. Seitz, W. Mittelmeier, R. Bader, Biomechanical behavior of bone scaffolds made of additive manufactured tricalciumphosphate and titanium alloy under different loading conditions. J Appl Biomater Funct Mater **11**, 159–166 (2013). https://doi.org/10.5301/JABFM.2013.10832
44. A. Reizabal, R. Brito-Pereira, M.M. Fernandes, N. Castro, V. Correia, C. Ribeiro, C.M. Costa, L. Perez, J.L. Vilas, S. Lanceros-Méndez, Silk fibroin magnetoactive nanocomposite films and membranes for dynamic bone tissue engineering strategies. Materialia **12**, 100709 (2020). https://doi.org/10.1016/j.mtla.2020.100709
45. Z. Montaseri, S.S. Abolmaali, A.M. Tamaddon, F. Farvadi, Composite silk fibroin hydrogel scaffolds for cartilage tissue regeneration. J Drug Deliv Sci Technol **79**, 104018 (2022). https://doi.org/10.1016/J.JDDST.2022.104018
46. H. Zhang, J. Han, Y. Sun, Y. Huang, M. Zhou, MC3T3-E1 cell response to stainless steel 316L with different surface treatments. Mater. Sci. Eng. C **56**, 22–29 (2015). https://doi.org/10.1016/j.msec.2015.06.017
47. A. Tevlek, S. Odabas, E. Çelik, H.M. Aydin, Preparation of MC3T3-E1 cell sheets through short-term osteogenic medium application. Artif Cells Nanomed Biotechnol **46**, 1145–1153 (2018). https://doi.org/10.1080/21691401.2018.1481081
48. W.B. Swanson, M. Omi, Z. Zhang, H.K. Nam, Y. Jung, G. Wang, P.X. Ma, N.E. Hatch, Y. Mishina, Macropore design of tissue engineering scaffolds regulates mesenchymal stem cell differentiation fate. Biomaterials **272**, 120769 (2021). https://doi.org/10.1016/J.BIOMATERIALS.2021.120769
49. S. Sprio, S. Panseri, M. Montesi, M. Dapporto, A. Ruffini, S.M. Dozio, R. Cavuoto, D. Misseroni, M. Paggi, D. Bigoni, A. Tampieri, Hierarchical porosity inherited by natural sources affects the mechanical and biological behaviour of bone scaffolds. J. Eur. Ceram. Soc. **40**, 1717–1727 (2020). https://doi.org/10.1016/J.JEURCERAMSOC.2019.11.015
50. P. Das, S. Ganguly, P.K. Marvi, M. Sherazee, S.R. Ahmed, X. Tang, S. Srinivasan, A.R. Rajabzadeh, Borophene based 3D extrusion printed nanocomposite hydrogel for antibacterial and controlled release application. Adv. Funct. Mater. (2024). https://doi.org/10.1002/ADFM.202314520